LANGMUIR

pubs.acs.org/Langmuir Article

Fabrication of Dandelion-like p−p Type Heterostructure of Ag_2O@CoO for Bifunctional Photoelectrocatalytic Performance

Lijun Yang, Yandong Hu, Mingming Su, and Lei Zhang*

Cite This: https://dx.doi.org/10.1021/acs.langmuir.0c02402 Read Online

ABSTRACT: A novel three-dimensional purple dandelion-like hierarchical Ag_2O@CoO heterojunction with an appropriate redox potential was constructed by chemical precipitation of Ag_2O nanoparticle on flower-like CoO. By feat of this hierarchical structure, the Ag_2O@CoO photocathode showed significantly high photoelectroreduction activities toward *p*-nitrophenol (*p*-NP) and Cr(VI). The high performance of Ag_2O@CoO was mainly attributed to the specific structural characteristics and synergistic effect of each chemical component. This hierarchical structure could effectively increase the specific surface area, provide more exposed active edges, and be beneficial for multiple light reflection/scattering channels and light utilization efficiency. The introduction of Ag_2O optimized the composition and further improved the band structure, resulting in an improved separation of photogenerated electrons and holes. The unique photocathode achieves a removal efficiency of 86% for photoelectrocatalytic *p*-NP degradation after 120 min and 95% for Cr(VI) after 40 min under visible light irradiation with excellent stability. This research provided a simple way for the synthesis of photoelectrocatalytic material with potential applications in the field of environmental governance with visible light illumination.

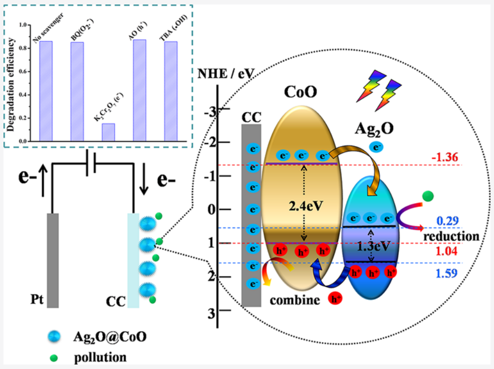

1. INTRODUCTION

Most organic compounds and heavy metal ions are common contaminants with long-term preservation, bioaccumulation, and high toxicity, which cannot be naturally degraded.[1−4] *p*-Nitrophenol (*p*-NP), a hydrolytic product from dyestuff, medicine, pesticide, and herbicide industries, may cause serious environmental problems and human health issues because of its toxicity, mutagenic potential, etc.[5−7] Chromium is a highly reactive metal, and Cr(VI) is more toxic than Cr(III), which can easily be absorbed and enriched in the human body, thus affecting the biological functions, and is extremely carcinogenic.[8] Rapid and complete treatment of contaminants in wastewater has become an issue of global concern. Most studies on the photocatalytic (PC) degradation of contaminants have been underlain by aqueous suspensions of semiconductor nanoparticles.[9−11] However, the difficulty of recycling powder semiconductor materials seriously limits their practical applications. Owing to the demand for environmental protection, as green technologies for solar to electricity energy, photoelectrocatalytic (PEC) degradation has attracted much attention compared with photocatalytic (PC) and electrocatalytic (EC) degradation recently,[12,13] mainly because of the efficient separation of photogenerated carriers with the external electric field. Meanwhile, it will avoid the secondary contamination of the aqueous environment by powder catalyst. So far, one of the major challenges of PEC is how to improve the utilization of solar energy and electricity. Therefore, developing an appropriate catalyst for PEC processes is significant.

Utilization of semiconducting materials as photoelectrodes toward contaminants opens new pathways in cost-effective generation of alternative photoelectrocatalysts. The semiconductor photosensitive electrode is the very key part in a PEC cell. Up to now, many metal oxide semiconductor photocatalysts, for instance, Cu_2O,[14] CuO,[15,16] CoO,[17,18] Co_3O_4,[19] TiO_2,[20] ZnO,[21−23] MnO_2,[24] WO_3,[25] NiO,[26] and Fe_2O_3,[27,28] have been synthesized for degrading hazardous contaminants. Among them, p-type CoO with many advantages such as the narrow energy band gap (2.2−2.6 eV),[17,18] high earth reserves, favorable price, and nontoxicity, has been widely used in energy conversion devices with high-efficiency visible light photocatalytic performances. Nevertheless, the short excited-state lifetime and high recombination rate of electron and hole often leads to unsatisfactory photoelectrochemical performances. Different efforts have been made to solve these problems, such as doping, adjusting

Received: August 13, 2020
Revised: September 22, 2020

Scheme 1. Schematic Illustration of the Preparation Process of 3D Purple Dandelion-like $Ag_2O@CoO$ Photoelectrode

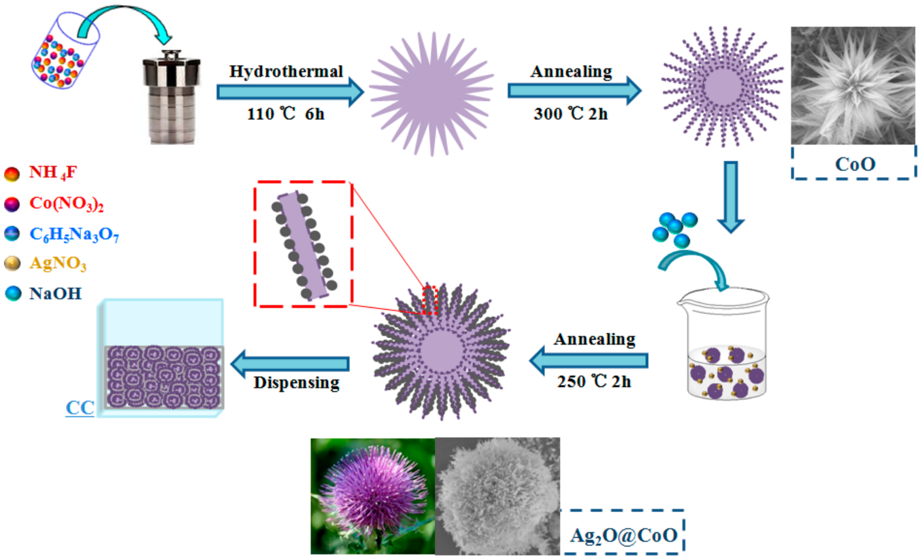

the morphology, decreasing the crystallite size, and constructing heterojunctions,[29] making them have high conductivity, high light utilization, and synergistic effects among components, ultimately leading to the enhanced separation efficiency of photoinduced electron−hole pairs and improved catalytic activity. Recently, various materials such as g-C_3N_4,[30,31] NiO,[32] TiO_2,[33,34] $SrTiO_3$,[35] and $CoSnO_3$[13] have been developed to construct heterojunctions for various PC and PEC applications. Silver oxide (Ag_2O) has ignited wide interest because of its excellent light response and conductivity.[36] However, individual Ag_2O with low quantum yield, poor light stability, and short life of charge carriers finally leads to poor photocatalytic activity. Therefore, Ag_2O is usually served as a cocatalyst, which exhibits a good photocatalytic activity in the decomposition of organic contaminant.[37−39] To our knowledge, there are no works published regarding the application of $Ag_2O@CoO$ p−p heterojunction on PEC degradation of organic and inorganic contaminants.

In this work, we develop a facile method to anchor Ag_2O nanoparticles on the nanoleaves of flower-like CoO to constitute a purple dandelion-like hierarchical $Ag_2O@CoO$ catalyst. The as-prepared hierarchical $Ag_2O@CoO$ has high specific surface area and multiple light reflection/scattering channels, which will provide more exposed active sites and higher light efficiency. The introduction of Ag_2O optimized the composition and the band structure of the as-prepared catalyst, and further improved the separation of photogenerated carriers, finally leading to a high removal capacity for pollutants. The as-prepared catalyst is active toward the reduction of *p*-nitrophenol (*p*-NP) and Cr(VI). Meanwhile, a possible mechanism for improving the activity of $Ag_2O@CoO$ is also proposed.

2. EXPERIMENTAL SECTION

2.1. Materials. $Co(NO_3)_2{\cdot}6H_2O$, NH_4F, urea, NaOH, $AgNO_3$, $C_6H_5Na_3O_7{\cdot}2H_2O$, *p*-nitrophenol (*p*-NP), and Cr(VI) are of analytical grade and were obtained from Sinopharm Chemical Reagent Co., Ltd. (China). Carbon paper was bought from Suzhou Dasheng Electronic Materials Co., Ltd. (China).

2.2. Preparation of Photoelectrocatalysts. *2.2.1. Preparation of CoO.* Three-dimensional hierarchical CoO flowers were synthesized by a solvothermal process according to our previous report:[13] 2 mmol of $Co(NO_3)_2{\cdot}6H_2O$, 10 mmol of urea and 2 mmol of NH_4F are dissolved in 50 mL of solution, and then the mixture is transferred into a 100 mL Teflon-lined steel autoclave and maintained at 110 °C for 6 h. The obtained precursor is collected and washed with deionized water and ethanol several times, then dried in oven at 60 °C for 8 h, and finally annealed at 300 °C for 2 h with a slow ramp rate of 2 °C min^{-1}.

2.2.2. Fabrication of 3D Purple Dandelion-like Hierarchical $Ag_2O@CoO$ Hybrid. A 30 mg sample of as-prepared CoO is dispersed in 20 mL of distilled water, and 15 mg of $AgNO_3$ is added into the above suspension. After 20 min of stirring, 20 mL of 0.06 M NaOH is slowly dropped into the above mixture until its pH reaches around 14. Finally, flower-like CoO coated with Ag_2O nanoparticles are washed thoroughly with distilled water followed by centrifugation and drying at 60 °C for 24 h, and finally annealed at 250 °C for 2 h with 2 °C min^{-1}. For comparison, pure Ag_2O nanoparticles are also synthesized by the same procedure without the addition of CoO.

2.3. Fabrication of $Ag_2O@CoO$ Electrode. The manufacturing process of 3D $Ag_2O@CoO$ photoelectrode is presented in Scheme 1. First, carbon paper (1 cm × 2 cm) was pretreated in line with the previous report.[13] Then 0.5 mL of 5 mg mL^{-1} $Ag_2O@CoO$ suspension is sonicated for 10 min and dropped onto the carbon paper (1 cm × 1 cm), and then the as-prepared electrode is dried at 60 °C for 12 h. For comparison, Ag_2O and CoO photoelectrodes are also constructed in a similar process with the same amount, thickness, and surface area.

2.4. Material Characterization. The morphology and microstructures of the as-prepared materials were examined with a scanning electron microscope (SEM; SU8000, Hitachi Co., Japan) operated at 10.0 kV. Transmission electron microscopy (TEM) was performed on a transmission electron microscope (TEM; 2100F, JEOL Co., Japan) with an accelerating voltage of 200 kV. Powder X-ray diffraction (XRD) patterns were collected on a diffractmeter (XRD; D8 Siemens Co., Germany), using Cu Kα radiation (λ = 0.1542 nm) in the 2θ range 10−80 with a scanning rate of 1 deg min^{-1}. The chemical state was analyzed by X-ray photoelectron spectroscopy (XPS) analysis performed on a Thermo Electron Corp. ESCALAB 250 Xi, and the binding energies were calibrated using the C 1s peak at 284.5 eV.

The photoelectrochemical properties are investigated with the use of a CHI660D electrochemical workstation (Shanghai Chenhua, China) with a standard three-electrode system equipped with the as-prepared electrode as the working electrode, Pt wire as the counter electrode, and Ag/AgCl as the reference electrode. The Mott−Schottky plots are collected with testing impedance spectra from −1.5 to 1.5 V. The current versus applied potential curve is obtained by sweeping the potential from 0 to −0.8 V at a scan rate of 5 mV s^{-1}.

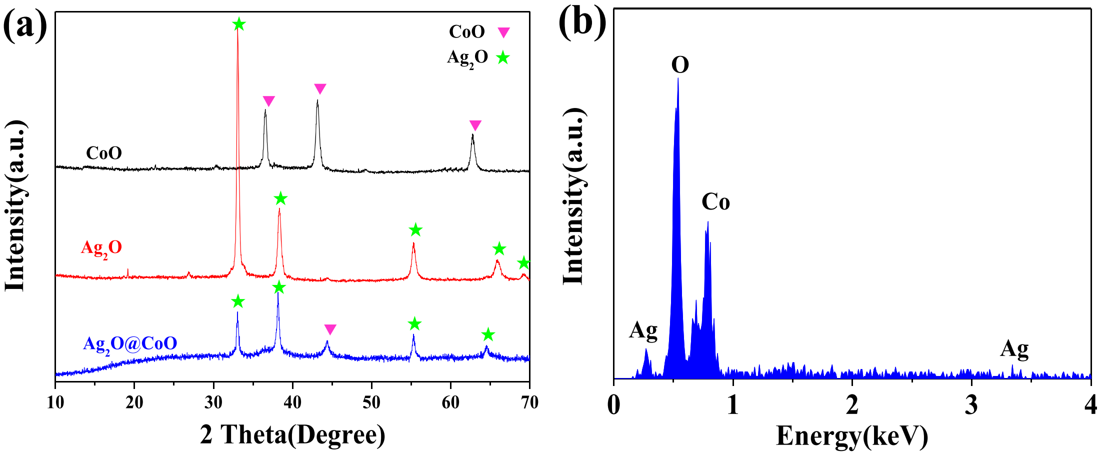

Figure 1. (a) XRD patterns of pristine CoO, Ag_2O, and Ag_2O@CoO. (b) EDX spectrum of Ag_2O@CoO.

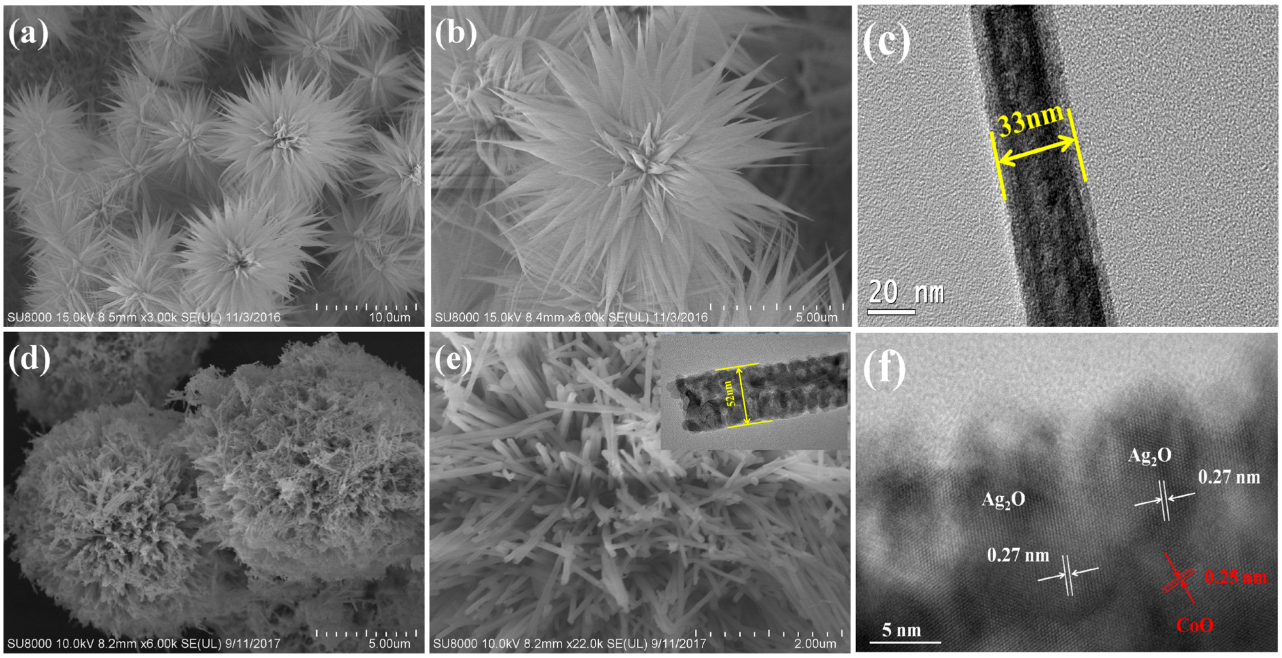

Figure 2. (a, b) SEM images of CoO. (c) TEM image of CoO branch. (d, e) SEM images of Ag_2O@CoO (inset in (e), TEM image of Ag_2O@CoO branch). (f) HRTEM image of Ag_2O@CoO.

The current−time curve is measured with periodical on/off visible light illumination (>420 nm) at −0.5 V bias. Electrochemical impedance spectra (EIS) are obtained by applying the open circuit potential (0.5 V) with 5 mV amplitude in a frequency range from 100 kHz to 1 Hz in 10 mmol L^{-1} $K_4[Fe(CN)_6]/K_3[Fe(CN)_6]$ containing 0.1 mol L^{-1} KCl. In the photoelectrochemical experiments, an adjustable 300 W Xe lamp (Beijing China Education Au-light Co. Ltd.) with a 420 nm cutoff filter serves as the light source. The potential versus Ag/AgCl is converted to the potential versus the normal hydrogen electrode (NHE) according to $E_{NHE} = E_{Ag/AgCl} + 0.2$ during analysis of the results.

2.5. Photoelectrocatalytic Activity Test. *p*-Nitrophenol (*p*-NP) and Cr(VI) ions are typical organic and inorganic contaminants, respectively, which are used as targets for evaluating the catalytic activities of the as-prepared catalysts with a 300 W xenon lamp (with a 420 nm cutoff filter) as the light source in this study. For electrocatalytic (EC) and photoelectrocatalytic (PEC) reactions, the as-prepared electrode as the working electrode was immersed into pH 3, 0.1 mol L^{-1} Na_2SO_4 electrolyte solution containing 10 mg L^{-1} *p*-NP/Cr(VI) and then magnetically stirred for 30 min in the dark to achieve an adsorption−desorption equilibrium before light irradiation. With the three-electrode system, the catalytic activities of the as-prepared electrode are evaluated under visible light irradiation with a cathode bias of −0.5 V vs SCE. For the photocatalytic (PC) reaction, 10 mg of the as-prepared photocatalyst was ultrasonically dispersed into pH 3, 0.1 mol L^{-1} Na_2SO_4 electrolyte solution containing 10 mg L^{-1} *p*-NP/Cr(VI) and then magnetically stirred in the dark for 30 min to achieve an adsorption−desorption equilibrium before light irradiation. During the reaction process, 3 mL of solution is taken out at regular time intervals and analyzed with a UV−vis absorption spectrometer to determine the residual amount of *p*-NP/Cr(VI) solution. After that, the 3 mL sample is promptly poured back into the reaction system after rapid measurement in order to reduce the impact of volume changes on the process.

3. RESULTS AND DISCUSSION

3.1. Structure Characterization. The phase and composition of the as-prepared heterostructure are examined by XRD and energy-dispersive spectroscopy (EDS) analysis. As shown in Figure 1a, the peaks located at 36.5, 42.4, and 61.5° can be indexed to the (111), (200), and (220) lattice planes of cubic CoO (JCPDS card no. 48-1719). After Ag_2O is anchored onto flower-like CoO arrays, the diffraction peaks at 32.5, 37.8, 54.5, and 64.9° can obviously be observed, which can be ascribed to the (111), (200), (220), and (311) crystal planes of cubic Ag_2O (JCPDS card no. 76-1393), revealing that Ag_2O nanoparticles have been successfully loaded on CoO. Furthermore, no traces of other peaks can be observed, confirming the high purity of CoO and Ag_2O. Also, the EDS spectrum of the composite (Figure 1b) further proved the presence of Co, Ag, and O and the high purity of the as-prepared materials.

The low-magnification SEM image (Figure 2a) reveals that the as-prepared CoO could be produced in large scale and exhibit high uniformity of 3D flower-like architectures assembled from dense nanoleaves. Figure 2b displays that flower-like CoO has a diameter of ~10 μm and the dense nanoleaves emanating from the center, which can provide amounts of open free space and sufficient active sites for anchoring Ag_2O and enlarging the contact area with the target. The length of the nanoleaf with sharp tips is in the range 1−5 μm, and the width is about 33 nm (Figure 2c). The porous structure of CoO can facilitate the transport of the target and ensure efficient contact between catalyst and target. As observed from Figure 2d, 3D Ag_2O@CoO exhibited a purple dandelion-like structure with a diameter of ~14 μm. Compared with the flower-like CoO, the diameter of Ag_2O@CoO has become bigger obviously after the introduction of Ag_2O. Further magnification of the SEM image (Figure 2e) reveals that the dandelion-like structure of Ag_2O@CoO is composed of many incompactly packed rough-surface nanoleaf structures (with a width of ~52 nm, inset in Figure 2e), which may further give rise to a larger surface and facilitate electron transfer. The TEM image inset in Figure 2e further confirms the formation of a heterojunction between CoO flower and Ag_2O nanoparticles, and many Ag_2O nanoparticles with diameters of 5−10 nm are tightly coupled on the surface of each leaf in an enlarged view. The HRTEM image (Figure 2f) exhibits crystalline lattices of 0.25 and 0.27 nm, corresponding to the (111) crystal plane of CoO and the (111) plane of Ag_2O, confirming the successful synthesis of 3D dandelion-like hierarchical Ag_2O@CoO heterojunction.

XPS experiment is used to confirm the elemental composition and valence states of the as-prepared Ag_2O@CoO hybrid. The typical XPS survey spectrum in Figure 3a demonstrates the presence of Co, Ag, O, and C elements. The Co 2p XPS spectrum is given in Figure 3b; two major peaks locked at 780.8 and 796.7 eV are assigned to Co $2p_{3/2}$ and Co $2p_{1/2}$, respectively, and two satellite peaks (abbreviated as "s") are also observed at 786.7 and 802.5 eV indicating the existence of Co^{2+}.[40,41] The doublet peaks located at 374.4 and 368.1 eV are assigned to Ag $3d_{3/2}$ and Ag $3d_{5/2}$, in accordance with the electronic state of Ag^+ in Ag_2O[42] (Figure 3c). The asymmetric O 1s XPS spectrum is deconvoluted into three symmetric peaks in Figure 3d. The peaks at 529.9 and 531.3 eV are ascribed to Co−O[18] and Ag−O bonds,[42] respectively, while the peak at 532.5 eV is associated with the chemisorbed oxygen caused by the external hydroxyl or the water molecules adsorbed on the surface of the composite.[43] Consequently, the above results confirm that Ag_2O nanoparticles are successfully anchored onto flower-like CoO.

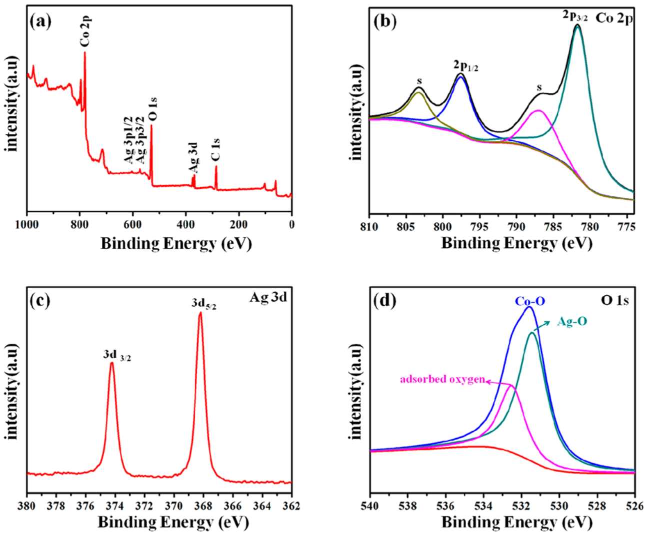

Figure 3. XPS spectra of Ag_2O@CoO: (a) survey, (b) Co 2p, (c) Ag 3d, and (d) O 1s.

3.2. Optical and Electrical Properties. To assess optical absorbance, UV−vis diffuse reflectance spectra (DRS) of Ag_2O, CoO, and Ag_2O@CoO are carried out and the results are shown in Figure 4a. As for the as-synthesized Ag_2O and CoO, both of them display strong light absorption in the range 200−800 nm, which is related to their outstanding visible photocatalytic activity. After Ag_2O nanoparticles are anchored onto the CoO branches, the absorption intensity is obviously improved as compared with single CoO from 400 to 800 nm. The data of DRS suggest that the construction of 3D hierarchical Ag_2O@CoO can increase the utilized efficiency of the solar light. The optical band gap energy (E_g) is assessed from the DRS spectra by use of a Tauc plot (Figure 4b). The band gap energy of Ag_2O@CoO is about 1.6 eV, which shows a decrease of the band gap compared with CoO (2.4 eV), and the decrease can be attributed to the nano dimension of Ag_2O anchored on flower-like CoO forming a heterojunction, which will facilitate the visible light absorption.[44−46] The flat-band potentials (E_{FB}) of the as-prepared photocatalysts were studied by Mott−Schottky plots in order to investigate the band-edge potentials of the conduction band (E_{CB}) and the valence band (E_{VB}). On the basis of the Mott−Schottky plots in Figure 4c, the negative slopes of the Mott−Schottky plots indicate that both CoO and Ag_2O are p-type semiconductors. The flat-band potential is determined to be 0.74 V (vs Ag/AgCl) for CoO, which equals 0.94 V (vs NHE). Meanwhile, the flat-band potential of Ag_2O is located at 1.29 eV versus Ag/AgCl (equivalent to 1.49 eV vs NHE). As reported, the flat band potential is 0.1−0.3 eV higher than E_{VB} in a p-type semiconductor.[30] Therefore, E_{VB} values for CoO and Ag_2O are estimated to be 1.04 and 1.59 V vs NHE, respectively. Additionaly, E_{CB} can be obtained by the formula $E_{CB} = E_{VB} - E_g$,[47−49] and then the E_{CB} values of CoO and Ag_2O are estimated to be −1.36 and 0.29 eV vs NHE, respectively.

3.3. Electrical Properties. To further study the photoelectrochemical response, a serious of tests including linear scan voltammetry, transient photocurrent response, and electrochemical impedance spectroscopy (EIS) are investigated in 0.1 mol L^{-1} Na_2SO_4 solution without any sacrificial reagents. Figure 5a shows the linear scan voltammograms of CoO, Ag_2O, and Ag_2O@CoO with light illumination in the potential range 0 to −0.8 V vs Ag/AgCl. It is found that Ag_2O@CoO exhibits a maximum photoresponse current density compared to CoO and Ag_2O at −0.5 V. The

https://dx.doi.org/10.1021/acs.langmuir.0c02402
Langmuir XXXX, XXX, XXX−XXX

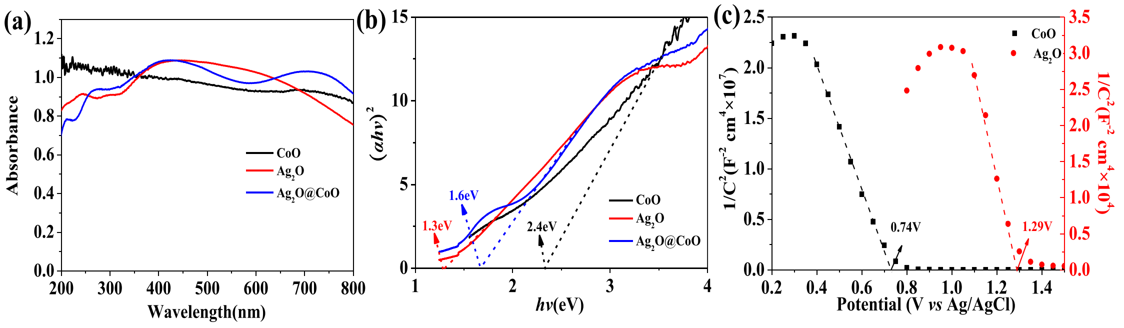

Figure 4. (a) UV−vis spectra. (b) Plots of $(\alpha h\nu)^2$ versus photon energy ($h\nu$). (c) Mott−Schottky plots.

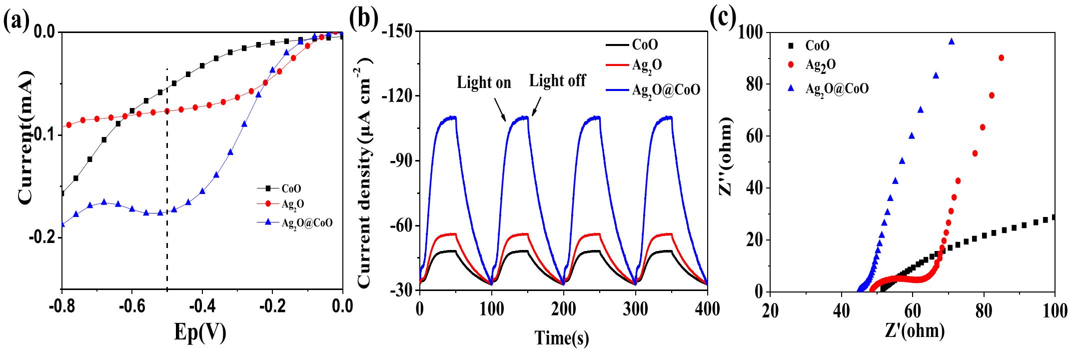

Figure 5. (a) $I-E_p$ curves under visible light illumination (>420 nm). (b) Photocurrent response to light on/off under visible light illumination (>420 nm) at −0.5 V vs Ag/AgCl. (c) Electrochemical impedance spectra (Nyquist plots) with open circuit potential (0.5 V vs Ag/AgCl) and 5 mV amplitude in a frequency range from 100 kHz to 1 Hz.

corresponding transient photocurrent responses are displayed in Figure 5b; the photocurrent is increased sharply under visible light irradiation but is promptly reduced to a minimum as soon as the irradiation decreases. Meanwhile, with light illumination the transient photocurrent of Ag_2O@CoO (73.77 μA cm^2) is 5.2 and 3.3 times higher than those of CoO (14.26 μA cm^2) and Ag_2O (22.62 μA cm^2), respectively, further suggesting that the p−p heterojunction can improve photoinduced charge transfer efficiency and highly promote the separation of photoinduced electrons and holes. Furthermore, the carrier density (N_d) can be obtained from the slope of the Mott−Schottky plot, according to eq 1:[21,22]

$$N_d = \frac{2}{\varepsilon \varepsilon_0 e_0}\left[\frac{d\frac{1}{C^2}}{dE}\right]^{-1} \tag{1}$$

where C is the specific capacity, ε is the dielectric constant of the material (10 for pristine CoO and Ag_2O), ε_0 is the permittivity of a vacuum (8.85 × 10^{-12} F·m^{-1}), e_0 is the electron charge (1.602 × 10^{-19} C), and E is the applied potential. Consequently, the carrier densities of CoO, Ag_2O, and Ag_2O@CoO are 2.45 × 10^{21}, 1.10 × 10^{23}, and 2.68 × 10^{23} cm^{-3}, respectively. The carrier density of Ag_2O@CoO increases about 109.4 times and 2.4 times compared to Ag_2O and CoO, respectively. The increased charge carrier density of Ag_2O@CoO indicates that the formation of p−p heterojunction is conducive to forming a sufficient space charge layer to promote the charge carrier transportation.

To further explore the catalytic kinetics and charge transfer performance, EIS Nyquist plots (Figure 5c) are investigated. In general, the smaller the radius of the arc in the EIS spectra, the higher charges transfer on the interface layer.[50,51] In Figure 5c, the circular radius of Ag_2O@CoO is smaller than those of the pure Ag_2O and CoO electrodes, indicating that 3D hierarchical Ag_2O@CoO has a faster interfacial charge transfer rate and lower mass transfer resistance. Therefore, it could be deduced that the interfacial charge transfer is accelerated due to the construction of Ag_2O@CoO p−p junction.

3.4. Photoelectrocatalytic Activity. The photoelectrocatalytic activities of the as-prepared electrodes are evaluated with a cathode bias of −0.5 V vs Ag/AgCl under visible light irradiation. Figure 6a clearly indicates that the PEC process is much more effective than EC and PC for the reduction of *p*-NP. The reduction efficiency reached nearly 86% after 120 min during the PEC process, while only 55% and 36% were obtained by PC and EC, respectively. The photochemical catalytic reduction performance of Ag_2O@CoO is also investigated. As shown in Figure 6b, the characteristic absorption peak of *p*-NP at 316 nm (the conjugation of benzene ring and chromophonic group)[52] dropped progressively in intensity with the proceeding of PEC reduction reaction without a sacrificial agent. Meanwhile, a new peak at 255 nm belonging to *p*-aminophenol (*p*-AP) arose and increased gradually, confirming the generation of *p*-AP. After 120 min of PEC reaction, the *p*-NP adsorption peak nearly disappeared, indicating that the hydrogenation reaction had proceeded completely with all *p*-NP converted into *p*-AP.

The linear relationship between the corresponding $\ln(C_0/C)$ and the reaction time is shown in Figure 6c, implying that the degradation reaction can be considered as a pseudo-first-order kinetics reaction. The kinetic constant (k) obtained from the slopes of their curves[53,54] decreases in the order Ag_2O@CoO

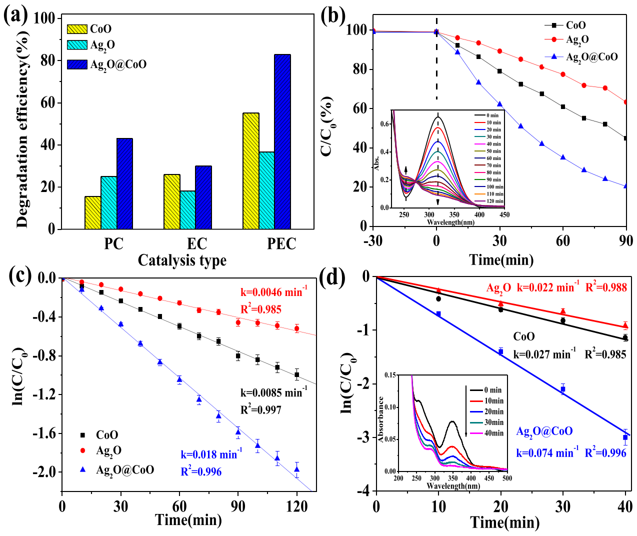

Figure 6. (a) PC, EC, and PEC degradation efficiencies of *p*-NP for different photoanodes. (b) PEC degradation of *p*-NP by different samples under visible light irradiation (inset, changes in UV−vis absorption spectra of *p*-NP aqueous solutions under PEC degradation). (c) Kinetic curves of PEC degradation of *p*-NP. (d) Kinetic curves of PEC reduction of Cr(VI) (inset, PEC degradation of Cr(VI) in UV−vis absorption spectra). Cathode bias, −0.5 V vs Ag/AgCl; visible light irradiation (>420 nm); 0.1 mol L^{-1} Na_2SO_4 (pH = 3); 10 mg L^{-1} target solution.

(0.018 min^{-1}) > CoO (0.0085 min^{-1}) > Ag_2O (0.0046 min^{-1}). Compared with pure CoO or Ag_2O, the estimated $k_{p\text{-NP}}$ on Ag_2O@CoO increased by ca. 2.1 or 3.9 times. The as-designed Ag_2O@CoO electrodes demonstrated excellent PEC reactivity for inorganic pollutant degradation, where an obvious synergetic effect between the PE and PC processes is observed. This synergetic effect could be due to the match of energy levels between Ag_2O and CoO.

The photoelectrocatalytic activities of as-prepared catalysts for Cr(VI) reduction are also conducted under visible light irradiation. Figure 6d clearly indicates that the reduction efficiency reached nearly 95% after 40 min in the PEC process. The results of the linear relation of $\ln(C/C_0)$ vs reaction time suggest that the reduction reaction of Cr(VI) can be regarded as a pseudo-first-order reaction (Figure 6d). The corresponding $k_{\mathrm{Cr(VI)}}$ of Ag_2O@CoO is calculated to be 0.074 min^{-1}, which is 2.9 and 3.4 times higher than those of CoO (0.02 min^{-1}) and Ag_2O (0.022 min^{-1}), respectively. The 3D purple dandelion-like hierarchical Ag_2O@CoO array is proved to be one of the ideal structures for photoelectroreduction of organic compounds and heavy metals.

The stability of Ag_2O@CoO electrode is studied by recycling tests. For each recycling test, Ag_2O@CoO electrode is washed with ethanol and deionized water three times, and the photocatalytic activity of Ag_2O@CoO electrode does not reduce significantly after three cycles (Figure 7a). Moreover, XRD analysis of the recycled Ag_2O@CoO shown in Figure 7b suggests its crystal structure has nearly no change and no impurity appears, confirming the excellent stability of Ag_2O@CoO during the PCE reaction.

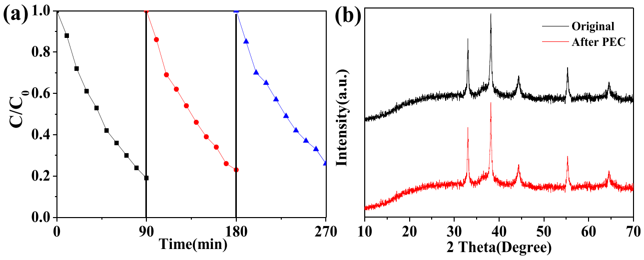

Figure 7. (a) Recyclability of PEC degradation of *p*-NP by Ag_2O@CoO photoanode under visible light illumination. (b) XRD patterns of Ag_2O@CoO before and after recycling test.

According to the above experiment results, the excellent PEC performance of Ag_2O@CoO photoelectrode can be explained as follows: 3D hierarchical CoO decorated with large amounts of Ag_2O nanoparticles with a higher specific surface area, more active sites, and matching band energy level alignment displays a superior light-harvesting efficiency for efficient charge collection, improves carrier generation and separation, and enhances organic pollutant absorption. Furthermore, the photogenerated electrons directly transport through the nanoleaf, which will provide an efficient electron transport pathway and further accelerate the collection of electrons and the separation of electrons−holes, ultimately improving the PEC activity of Ag_2O@CoO.

3.5. Mechanism. In the PEC process of Ag_2O@CoO, the introduced Ag_2O can significantly enhance the photoelectrocatalytic activity of CoO through the enhanced charge separation under additional bias voltage and visible light irradiation. Owing to 3D purple dandelion-like structural features, it provides effective electron transport pathways, high specific surface area, more reactive sites, and high light-harvesting efficiency.[55−57] The mechanism of the charge separation is shown in Scheme 2. Both Ag_2O and CoO are very typical p-type narrow band gap semiconductors, and they can be easily excited under visible light irradiation to generate photoelectrons and holes. As shown, the E_{CB} of CoO is of a more negative potential (−1.36 eV) than that of Ag_2O (0.29 eV), which will cause the photogenerated electrons to migrate from the conduction band of CoO to that of Ag_2O. In contrast, the holes will transfer from the valence band of Ag_2O to that of CoO because the E_{VB} of Ag_2O is of a more positive potential than that of CoO.[58−62] Therefore, the transfer of these charge carriers will result in the accumulation of the photogenerated

Scheme 2. Possible PEC Degradation Mechanism for 3D Ag_2O@CoO under Visible Light Illumination (Inset, Trapping Experiments)

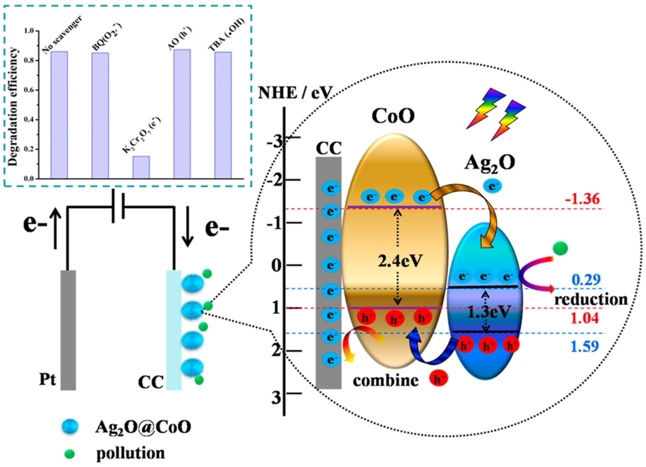

electrons on the CB of Ag_2O and the photogenerated holes on the VB of CoO. The accumulated electrons on the CB of Ag_2O will eventually achieve the photocatalytic reduction of *p*-NP and Cr(IV). Meanwhile, holes in the VB of CoO are scavenged by the electrons from the carbon cloth to generate a cathode photocurrent, and the large cathode photocurrent of Ag_2O@CoO electrode (Figure 5a) reveals that amounts of photogenerated holes flow to the cathode via the external circuit and the photogenerated electrons are left on the photoelectrode for photoelectrocatalytic reduction.

4. CONCLUSION

In this work, a 3D purple dandelion-like hierarchical Ag_2O@CoO has been successfully designed and fabricated, and it showed improved photoelectroreduction activities toward *p*-nitrophenol and Cr(VI) as a photocathode. The improved photoelectrocatalytic perfomance of Ag_2O@CoO is attributed to the 3D purple dandelion-like hierarchical structure and synergistic effects of each component. The unique hierarchical structure with high specific surface area will provide more exposed active sites, multiple light reflection/scattering channels, superior light-harvesting efficiency, and improved diffusion kinetics. Meanwhile, Ag_2O as cocatalyst will adjust the chemical composition, optimize the band structure, and accelerate the separation of photogenerated electrons and holes, ultimately leading to an improved photoelectrocatalytic activity for pollutants. This research demonstrates that the as-prepared Ag_2O@CoO photoelectrode has great potential applications in the field of PEC for treatment of wastewater contaminants.

AUTHOR INFORMATION

Corresponding Author

Lei Zhang − *College of Chemistry, Liaoning University, Shenyang, Liaoning 110036, People's Republic of China;* orcid.org/0000-0001-7584-0184; Phone: +86 24 62207809; Email: zhanglei63@126.com; Fax: +86 24 62202380

Authors

Lijun Yang − *College of Chemistry, Liaoning University, Shenyang, Liaoning 110036, People's Republic of China*
Yandong Hu − *College of Chemistry, Liaoning University, Shenyang, Liaoning 110036, People's Republic of China*
Mingming Su − *Dalian Customs District, Dalian, Liaoning 116000, People's Republic of China*

Complete contact information is available at:
https://pubs.acs.org/10.1021/acs.langmuir.0c02402

Author Contributions

L.Y., conceptualization, methodology, data curation, formal analysis, writing—original draft preparation; Y.H., methodology, investigation, writing—original draft preparation; M.S., visualization, data curation; L.Z., funding acquisition, writing—reviewing and editing.

Notes

The authors declare no competing financial interest.

ACKNOWLEDGMENTS

This work was financially supported by the National Natural Science Foundation of China (NSFC 51672116) and Liao Ning Revitalization Talents Program (XLYC1902066).

REFERENCES

(1) Xia, J.; He, G.; Zhang, L.; Sun, X.; Wang, X. Hydrogenation of nitrophenols catalyzed by carbon black-supported nickel nanoparticles under mild conditions. *Appl. Catal., B* **2016**, *180*, 408−415.

(2) Hasan, Z.; Cho, D. W.; Chon, C. M.; Yoon, K.; Song, H. Reduction of p-nitrophenol by magnetic Co-carbon composites derived from metal organic frameworks. *Chem. Eng. J.* **2016**, *298*, 183−190.

(3) Yang, L.; Zheng, X.; Liu, M.; Luo, S.; Luo, Y.; Li, G. Fast photoelectro-reduction of Cr(VI) over MoS_2@TiO_2 nanotubes on Ti wire. *J. Hazard. Mater.* **2017**, *329*, 230−240.

(4) Yang, L.; Zhang, Y.; Liu, X.; Jiang, X.; Zhang, Z.; Zhang, T.; Zhang, L. The investigation of synergistic and competitive interaction between dye Congo red and methyl blue on magnetic $MnFe_2O_4$. *Chem. Eng. J.* **2014**, *246*, 88−96.

(5) Nezamzadeh-Ejhieh, A.; Amiri, M. CuO supported Clinoptilolite towards solar photocatalytic degradation of p-aminophenol. *Powder Technol.* **2013**, *235*, 279−288.

(6) Nezamzadeh-Ejhieh, A.; Khorsandi, S. Photocatalytic degradation of 4-nitrophenol with ZnO supported nano-clinoptilolite zeolite. *J. Ind. Eng. Chem.* **2014**, *20* (3), 937−946.

(7) Soori, F.; Nezamzadeh-Ejhieh, A. Synergistic effects of copper oxide-zeolite nanoparticles composite on photocatalytic degradation of 2,6-dimethylphenol aqueous solution. *J. Mol. Liq.* **2018**, *255*, 250−256.

(8) Nezamzadeh-Ejhieh, A.; Shahanshahi, M. Modification of clinoptilolite nano-particles with hexadecylpyridynium bromide surfactant as an active component of Cr(VI) selective electrode. *J. Ind. Eng. Chem.* **2013**, *19* (6), 2026−2033.

(9) Kumar, S. G.; Rao, K. S. R. K. Comparison of modification strategies towards enhanced charge carrier separation and photocatalytic degradation activity of metal oxide semiconductors (TiO_2, WO_3 and ZnO). *Appl. Surf. Sci.* **2017**, *391*, 124−148.

(10) Miller, E. B.; Zahran, E. M.; Knecht, M. R.; Bachas, L. G. Metal oxide semiconductor nanomaterial for reductive debromination: Visible light degradation of polybrominated diphenyl ethers by Cu_2O@Pd nanostructures. *Appl. Catal., B* **2017**, *213*, 147−154.

(11) Xiao, X.; Tu, S.; Lu, M.; Zhong, H.; Zheng, C.; Zuo, X.; Nan, J. Discussion on the reaction mechanism of the photocatalytic degradation of organic contaminants from a viewpoint of semiconductor photo-induced electrocatalysis. *Appl. Catal., B* **2016**, *198*, 124−132.

(12) Yang, L.; Hu, Y.; Zhang, L. Architecting Z-scheme Bi_2S_3@CoO with 3D chrysanthemums-like architecture for both photoeletro-oxidization and-reduction performance under visible light. *Chem. Eng. J.* **2019**, *378*, 122092.

(13) Zhang, L.; Hu, Y.; Zheng, J. Fabrication of 3D hierarchical $CoSnO_3$@CoO pine needle-like array photoelectrode for enhanced photoelectrochemical properties. *J. Mater. Chem. A* **2017**, *5* (35), 18664−18673.

(14) Omrani, N.; Nezamzadeh-Ejhieh, A. Focus on scavengers' effects and GC-MASS analysis of photodegradation intermediates of sulfasalazine by Cu_2O/CdS nanocomposite. *Sep. Purif. Technol.* **2020**, *235*, 116228.

(15) Gusain, R.; Kumar, P.; Sharma, O. P.; Jain, S. L.; Khatri, O. P. Reduced graphene oxide−CuO nanocomposites for photocatalytic conversion of CO_2 into methanol under visible light irradiation. *Appl. Catal., B* **2016**, *181*, 352−362.

(16) Lei, M.; Wang, N.; Zhu, L.; Zhou, Q.; Nie, G.; Tang, H. Photocatalytic reductive degradation of polybrominated diphenyl ethers on CuO/TiO_2 nanocomposites: A mechanism based on the switching of photocatalytic reduction potential being controlled by the valence state of copper. *Appl. Catal., B* **2016**, *182*, 414−423.

(17) Liu, B.; Ma, L.; Ning, L. C.; Zhang, C. J.; Han, G. P.; Pei, C. J.; Zhao, H.; Liu, S. Z.; Yang, H. Q. Charge Separation between Polar {111} Surfaces of CoO Octahedrons and Their Enhanced Visible-Light Photocatalytic Activity. *ACS Appl. Mater. Interfaces* **2015**, *7*, 6109−6117.

(18) Shi, W.; Guo, F.; Wang, H.; Han, M.; Li, H.; Yuan, S.; Huang, H.; Liu, Y.; Kang, Z. Carbon dots decorated the exposing high-reactive (111) facets CoO octahedrons with enhanced photocatalytic activity and stability for tetracycline degradation under visible light irradiation. *Appl. Catal., B* **2017**, *219*, 36−44.

(19) Liu, J.; Wang, D.; Wang, M.; Kong, D.; Zhang, Y.; Chen, J. F.; Dai, L. Uniform Two-Dimensional Co_3O_4 Porous Sheets: Facile Synthesis and Enhanced Photocatalytic Performance. *Chem. Eng. Technol.* **2016**, *39* (5), 891−898.

(20) Khanchandani, S.; Kumar, S.; Ganguli, A. K. Comparative Study of TiO_2/CuS Core/Shell and Composite Nanostructures for Efficient Visible Light Photocatalysis. *ACS Sustainable Chem. Eng.* **2016**, *4* (3), 1487−1499.

(21) Wei, R.; Kuang, P.; Cheng, H.; Chen, Y.; Long, J.; Zhang, M.; Liu, Z. Plasmon-Enhanced Photoelectrochemical Water Splitting on Gold Nanoparticle Decorated ZnO-CdS Nanotube Arrays. *ACS Sustainable Chem. Eng.* **2017**, *5*, 4249−4257.

(22) Liu, Z.; Kuang, P.; Wei, R.; Li, N.; Chen, Y.; Su, Y. BiOBr nanoplate-wrapped ZnO nanorod arrays for high performance photoelectrocatalytic application. *RSC Adv.* **2016**, *6*, 16122−16130.

(23) Noruozi, A.; Nezamzadeh-Ejhieh, A. Preparation, characterization, and investigation of the catalytic property of α-Fe_2O_3-ZnO nanoparticles in the photodegradation and mineralization of methylene blue. *Chem. Phys. Lett.* **2020**, *752*, 137587.

(24) He, S.; Xiao, K.; Chen, X.-Z.; Li, T.; Ouyang, T.; Wang, Z.; Guo, M.-L.; Liu, Z.-Q. Enhanced photoelectrocatalytic activity of direct Z-scheme porous amorphous carbon nitride/manganese dioxide nanorod arrays. *J. Colloid Interface Sci.* **2019**, *557*, 644−654.

(25) Newton, K. A.; Osterloh, F. E. Size and Morphology of Suspended WO_3 Particles Control Photochemical Charge Carrier Extraction and Photocatalytic Water Oxidation Activity. *Top. Catal.* **2016**, *59* (8−9), 750−756.

(26) Gnanasekaran, L.; Hemamalini, R.; Saravanan, R.; Ravichandran, K.; Gracia, F.; Agarwal, S.; Gupta, V. K. Synthesis and characterization of metal oxides (CeO_2, CuO, NiO, Mn_3O_4, SnO_2 and ZnO) nanoparticles as photo catalysts for degradation of textile dyes. *J. Photochem. Photobiol., B* **2017**, *173*, 43−49.

(27) He, S.; Yan, C.; Chen, X.-Z.; Wang, Z.; Ouyang, T.; Guo, M.-L.; Liu, Z.-Q. Construction of core-shell heterojunction regulating α-Fe_2O_3 layer on CeO_2 nanotube arrays enables highly efficient Z-scheme photoelectrocatalysis. *Appl. Catal., B* **2020**, *276*, 119138.

(28) Zheng, B.-F.; Ouyang, T.; Wang, Z.; Long, J.; Chen, Y.; Liu, Z.-Q. Enhanced plasmon-driven photoelectrocatalytic methanol oxidation on Au decorated α-Fe_2O_3 nanotube arrays. *Chem. Commun.* **2018**, *54* (69), 9583−9586.

(29) Derikvandi, H.; Nezamzadeh-Ejhieh, A. Increased photocatalytic activity of NiO and ZnO in photodegradation of a model drug aqueous solution: Effect of coupling, supporting, particles size and calcination temperature. *J. Hazard. Mater.* **2017**, *321*, 629−638.

(30) Guo, F.; Shi, W.; Wang, H.; Han, M.; Li, H.; Huang, H.; Liu, Y.; Kang, Z. Facile fabrication of a CoO/g-C_3N_4 p−n heterojunction with enhanced photocatalytic activity and stability for tetracycline degradation under visible light. *Catal. Sci. Technol.* **2017**, *7* (15), 3325−3331.

(31) Mao, Z.; Chen, J.; Yang, Y.; Wang, D.; Bie, L.; Fahlman, B. D. Novel g-C_3N_4/CoO Nanocomposites with Significantly Enhanced Visible-Light Photocatalytic Activity for H2 Evolution. *ACS Appl. Mater. Interfaces* **2017**, *9*, 12427−12435.

(32) Zhao, Y.; Zhang, Y.; Ding, Y.; Chen, M. Hexagonal nanoplates of NiO/CoO/Fe_2O_3 composite acting as an efficient photocatalytic and electrocatalytic water oxidation catalyst. *Dalton Transactions* **2015**, *44* (35), 15628−15635.

(33) Savio, A. K. P. D.; Fletcher, J.; Smith, K.; Iyer, R.; Bao, J. M.; Robles Hernández, F. C. Environmentally effective photocatalyst CoO−TiO_2 synthesized by thermal precipitation of Co in amorphous TiO_2. *Appl. Catal., B* **2016**, *182*, 449−455.

(34) Yan, J.; Yang, S.; Xie, Z.; Li, X.; Zhou, W.; Zhang, X.; Fang, Y.; Zhang, S.; Peng, F. Heterostructured CoO/3D-TiO_2 nanorod arrays for photoelectrochemical water splitting hydrogen production. *J. Solid State Electrochem.* **2017**, *21* (2), 455−461.

(35) Qin, Y.; Wang, G.; Wang, Y. Study on the photocatalytic property of La-doped CoO/$SrTiO_3$ for water decomposition to hydrogen. *Catal. Commun.* **2007**, *8* (6), 926−930.

(36) Guo, H.; Niu, H.-Y.; Liang, C.; Niu, C.-G.; Huang, D.-W.; Zhang, L.; Tang, N.; Yang, Y.; Feng, C.-Y.; Zeng, G.-M. Insight into the energy band alignment of magnetically separable Ag_2O/$ZnFe_2O_4$ p-n heterostructure with rapid charge transfer assisted visible light photocatalysis. *J. Catal.* **2019**, *370*, 289−303.

(37) Wang, X.; Li, S.; Yu, H.; Yu, J.; Liu, S. Ag_2O as a new visible-light photocatalyst: self-stability and high photocatalytic activity. *Chem. - Eur. J.* **2011**, *17* (28), 7777−7780.

(38) Wang, G.; Ma, X.; Huang, B.; Cheng, H.; Wang, Z.; Zhan, J.; Qin, X.; Zhang, X.; Dai, Y. Controlled synthesis of Ag_2O microcrystals with facet-dependent photocatalytic activities. *J. Mater. Chem.* **2012**, *22* (39), 21189−21194.

(39) Karimi-Shamsabadi, M.; Nezamzadeh-Ejhieh, A. Comparative study on the increased photoactivity of coupled and supported manganese-silver oxides onto a natural zeolite nano-particles. *J. Mol. Catal. A: Chem.* **2016**, *418−419*, 103−114.

(40) Bai, J.; Wang, K.; Feng, J.; Xiong, S. ZnO/CoO and $ZnCo_2O_4$ Hierarchical Bipyramid Nanoframes: Morphology Control, Formation Mechanism, and Their Lithium Storage Properties. *ACS Appl. Mater. Interfaces* **2015**, *7*, 22848−22857.

(41) Chang, L.; Wang, K.; Huang, L.; He, Z.; Zhu, S.; Chen, M.; Shao, H.; Wang, J. Hierarchical CoO microflower film with excellent electrochemical lithium/sodium storage performance. *J. Mater. Chem. A* **2017**, *5*, 20892−20902.

(42) Chen, Y.; Zhu, G.; Hojamberdiev, M.; Gao, J.; Zhu, R.; Wang, C.; Wei, X.; Liu, P. Three-dimensional Ag_2O/Bi_5O_7I p-n heterojunction photocatalyst harnessing UV-vis-NIR broad spectrum for photodegradation of organic pollutants. *J. Hazard. Mater.* **2018**, *344*, 42−54.

(43) Liu, Y.; Zhu, G.; Gao, J.; Zhu, R.; Hojamberdiev, M.; Wang, C.; Wei, X.; Liu, P. A novel synergy of Er^{3+}/Fe^{3+} co-doped porous Bi_5O_7I microspheres with enhanced photocatalytic activity under visible-light irradiation. *Appl. Catal., B* **2017**, *205*, 421−432.

(44) Azimi, S.; Nezamzadeh-Ejhieh, A. Enhanced activity of clinoptilolite-supported hybridized PbS−CdS semiconductors for the photocatalytic degradation of a mixture of tetracycline and cephalexin aqueous solution. *J. Mol. Catal. A: Chem.* **2015**, *408*, 152−160.

(45) Jafari, S.; Nezamzadeh-Ejhieh, A. Supporting of coupled silver halides onto clinoptilolite nanoparticles as simple method for increasing their photocatalytic activity in heterogeneous photodegradation of mixture of 4-methoxy aniline and 4-chloro-3-nitro aniline. *J. Colloid Interface Sci.* **2017**, *490*, 478−487.

(46) Derikvandi, H.; Nezamzadeh-Ejhieh, A. Designing of experiments for evaluating the interactions of influencing factors on the photocatalytic activity of NiS and SnS_2: Focus on coupling, supporting and nanoparticles. *J. Colloid Interface Sci.* **2017**, *490*, 628−641.

(47) Omrani, N.; Nezamzadeh-Ejhieh, A. A comprehensive study on the mechanism pathways and scavenging agents in the photocatalytic activity of $BiVO_4$/WO_3 nano-composite. *Journal of Water Process Engineering* **2020**, *33*, 101094.

(48) Omrani, N.; Nezamzadeh-Ejhieh, A. A ternary Cu_2O/$BiVO_4$/WO_3 nano-composite: Scavenging agents and the mechanism pathways in the photodegradation of sulfasalazine. *J. Mol. Liq.* **2020**, *315*, 113701.

(49) Omrani, N.; Nezamzadeh-Ejhieh, A. $BiVO_4$/WO_3 nano-composite: characterization and designing the experiments in photodegradation of sulfasalazine. *Environ. Sci. Pollut. Res.* **2020**, DOI: 10.1007/s11356-020-10278-1.

(50) Nosuhi, M.; Nezamzadeh-Ejhieh, A. High catalytic activity of Fe(II)-clinoptilolite nanoparticales for indirect voltammetric determination of dichromate: Experimental design by response surface methodology (RSM). *Electrochim. Acta* **2017**, *223*, 47−62.

(51) Senobari, S.; Nezamzadeh-Ejhieh, A. A p−n junction NiO-CdS nanoparticles with enhanced photocatalytic activity: A response surface methodology study. *J. Mol. Liq.* **2018**, *257*, 173−183.

(52) Lai, B.; Zhang, Y.; Chen, Z.; Yang, P.; Zhou, Y.; Wang, J. Removal of p-nitrophenol (PNP) in aqueous solution by the micron-scale iron−copper (Fe/Cu) bimetallic particles. *Appl. Catal., B* **2014**, *144*, 816−830.

(53) Nezamzadeh-Ejhieh, A.; Hushmandrad, S. Solar photo-decolorization of methylene blue by CuO/X zeolite as a heterogeneous catalyst. *Appl. Catal., A* **2010**, *388* (1), 149−159.

(54) Shams-Ghahfarokhi, Z.; Nezamzadeh-Ejhieh, A. As-synthesized ZSM-5 zeolite as a suitable support for increasing the photoactivity of semiconductors in a typical photodegradation process. *Mater. Sci. Semicond. Process.* **2015**, *39*, 265−275.

(55) Liu, X.; Xu, D.; Zhang, D.; Zhang, G.; Zhang, L. Superior performance of 3D Co-Ni bimetallic oxides for catalytic degradation of organic dye: Investigation on the effect of catalyst morphology and catalytic mechanism. *Appl. Catal., B* **2016**, *186*, 193−203.

(56) Cui, W.; An, W.; Liu, L.; Hu, J.; Liang, Y. Novel Cu_2O quantum dots coupled flower-like BiOBr for enhanced photocatalytic degradation of organic contaminant. *J. Hazard. Mater.* **2014**, *280*, 417−427.

(57) Chang, F.; Xie, Y.; Chen, J.; Luo, J.; Li, C.; Hu, X.; Xu, B. Template-free synthesis and enhanced photocatalytic performance of uniform BiOCl flower-like microspheres. *J. Nanosci. Nanotechnol.* **2015**, *15* (2), 1421−1426.

(58) Amiri, M.; Nezamzadeh-Ejhieh, A. Improvement of the photocatalytic activity of cupric oxide by deposition onto a natural clinoptilolite substrate. *Mater. Sci. Semicond. Process.* **2015**, *31*, 501−508.

(59) Senobari, S.; Nezamzadeh-Ejhieh, A. A comprehensive study on the enhanced photocatalytic activity of CuO-NiO nanoparticles: Designing the experiments. *J. Mol. Liq.* **2018**, *261*, 208−217.

(60) Ghattavi, S.; Nezamzadeh-Ejhieh, A. A visible light driven AgBr/g-C_3N_4 photocatalyst composite in methyl orange photodegradation: Focus on photoluminescence, mole ratio, synthesis method of g-C_3N_4 and scavengers. *Composites, Part B* **2020**, *183*, 107712.

(61) Ghattavi, S.; Nezamzadeh-Ejhieh, A. GC-MASS detection of methyl orange degradation intermediates by AgBr/g-C_3N_4: Experimental design, bandgap study, and characterization of the catalyst. *Int. J. Hydrogen Energy* **2020**, *45* (46), 24636−24656.

(62) Mirsalari, S. A.; Nezamzadeh-Ejhieh, A. Focus on the photocatalytic pathway of the CdS-AgBr nano-catalyst by using the scavenging agents. *Sep. Purif. Technol.* **2020**, *250*, 117235.